Dispersion measurement of microstructured negative curvature hollow core fiber

Optical Engineering

OpticalEngineering.SPIEDigitalLibrary.org

Dispersion measurement of microstructured negative curvature hollow core fiber

Richard M. Carter
William N. MacPherson
Piotr Jaworski
Fei Yu
Rainer Beck
Jonathan D. Shephard
Duncan P. Hand

SPIE.

Richard M. Carter, William N. MacPherson, Piotr Jaworski, Fei Yu, Rainer Beck, Jonathan D. Shephard, Duncan P. Hand, "Dispersion measurement of microstructured negative curvature hollow core fiber," *Opt. Eng.* **55**(11), 116106 (2016), doi: 10.1117/1.OE.55.11.116106.

Dispersion measurement of microstructured negative curvature hollow core fiber

Richard M. Carter,[a,*] William N. MacPherson,[a] Piotr Jaworski,[a] Fei Yu,[b] Rainer Beck,[a] Jonathan D. Shephard,[a] and Duncan P. Hand[a]
[a]Heriot-Watt University, Institute of Photonics and Quantum Sciences, David Brewster Building, Edinburgh EH14 4AS, United Kingdom
[b]University of Bath, Centre for Photonics and Photonic Materials, Department of Physics, Bath BA2 7AY, United Kingdom

Abstract. We present measurements of the dispersion of two negative curvature fibers at and around 1 μm. These fibers are suitable for beam delivery of both high power and ultrashort pulse lasers with one designed to operate at 1030 nm and the other designed for dual wavelength delivery at 515 and 1030 nm. Both fibers were found to exhibit anomalous dispersion measured to be 2.17 ± 0.25 ps nm^{-1} km^{-1} for the fundamental mode rising to 4.69 ± 0.17 ps nm^{-1} km^{-1} for the first-order mode in the 1030-nm fiber. Dispersion in the double wavelength fiber was found to be higher at 3.81 ± 0.03 ps nm^{-1} km^{-1} for the fundamental mode guiding at 1030 nm. [DOI: 10.1117/1.OE.55.11.116106]

Keywords: fiber characterization; microstructured fiber; pulse propagation.

Paper 161357 received Aug. 30, 2016; accepted for publication Oct. 24, 2016; published online Nov. 17, 2016.

1 Introduction

Ultrafast short pulsed (10 ps and shorter) lasers are increasingly used in a range of industrial and experimental areas that should benefit from flexible beam delivery systems over distances of a few meters, i.e., optical fiber; however, for fiber optic delivery of high peak power, ultrafast pulsed lasers are principally limited by either maximum energy densities or through fiber dispersion. In addition, there has been recent interest in hollow core fiber for low latency and ultralow loss telecommunication applications over longer kilometer scales.[1]

Over the last few years, large mode area solid core and hollow core photonic crystal fibers have been presented as possible solutions to this fiber delivery problem.[2–5] Neither, however, presents a complete solution to the problems of damage threshold and dispersion.[2,3,5] Recently new designs of hollow core fibers, principally Kagomi fibers and negative curvature fibers (NCFs), have been proposed.[6–16] Although there has been considerable interest in developing these fiber designs, there have been, to date, limited direct measurement of the dispersion of these fiber designs.[17,18]

In this paper, we directly measure the dispersion of two hollow core NCFs at around 1 μm, a wavelength suitable for a range of machining applications that have been demonstrated with such fibers.[10,11]

2 Negative Curvature Fiber

An NCF is a hollow core fiber guiding through the antiresonance reflecting optical waveguide principle.[19] In essence, the core walls act as a Fabrey–Pérot cavity. Wavelengths in antiresonance with the core walls destructively interfere in transmission and are reflected back into the core providing confinement. Resonant wavelengths by comparison are transmitted from the core into the cladding and lost. Here, the wall thickness is critical to guidance and for operation at 1030 nm is of the order of 910 ± 50 nm.

An idealized structure for this form of fiber (for guidance at around 1 μm) is an unsupported 910 nm capillary. This is not practical since a manufactured design requires a supporting structure. This structure includes nodes where supporting struts attach to the core walls. These nodes can themselves support highly lossy modes and, in order to reduce these losses, are pushed away from the guided mode by using negatively curved core walls.

Dispersion measurements of two fibers are presented in this paper. Both fibers were manufactured at the University of Bath and scanning electron microscope (SEM) images are presented in Fig. 1. One is designed to operate with the first-order transmission band around 1030 nm. For this fiber, the comparatively large core (~38 μm) of the fiber supports a small number (<4) of low attenuation core modes and as such is not pure single mode at either 1030 or 1064 nm. This fiber is similar to the fiber presented in Ref. 11; however, it is further optimized with an attenuation of 0.037 and 0.031 dB m^{-1} at 1030 and 1064 nm, respectively (Fig. 2). This fiber is referred to as the first-order NCF.

The second fiber was designed to guide with a first-order transmission band at ~515 nm. As a result, the fiber has a zero-order transmission band at 1064 nm. Due to the smaller core size (~15 μm), this fiber can operate as a single mode at 1064 nm. Further details on this fiber operating in the green, and, in particular, the bend sensitivity can be found in Ref. 10. For the purposes of this paper, it is enough to note that the attenuation at 1064 nm is somewhat higher at 0.174 dB m^{-1} (Fig. 3) and that the transmission window is not smooth. This fiber is referred to as the zero-order NCF.

*Address all correspondence to: Richard M. Carter, E-mail: r.m.carter@hw.ac.uk

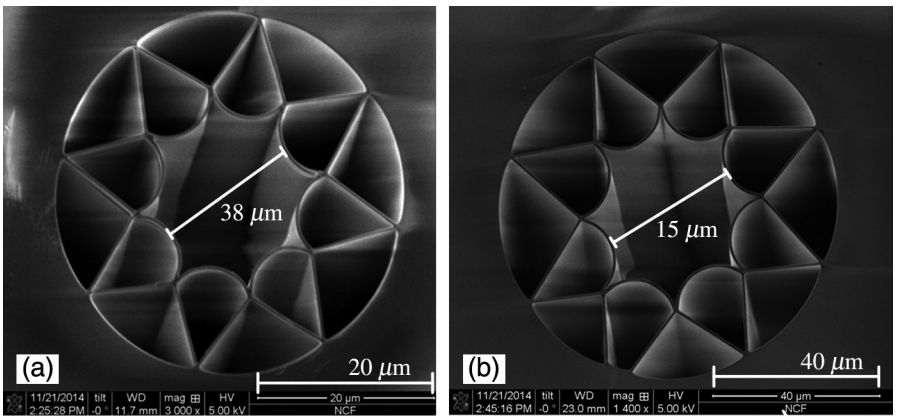

Fig. 1 SEM images of the NCFs used in this experiment: (a) 515 nm designed fiber and (b) 1030 nm designed fiber.

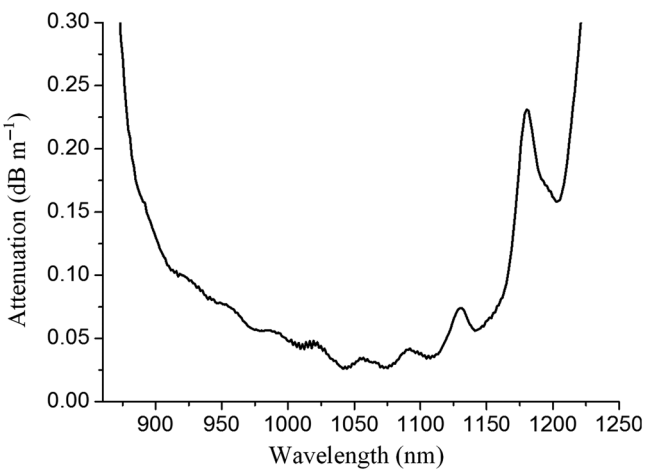

Fig. 2 Attenuation spectrum of first-order NCF presented in this paper.

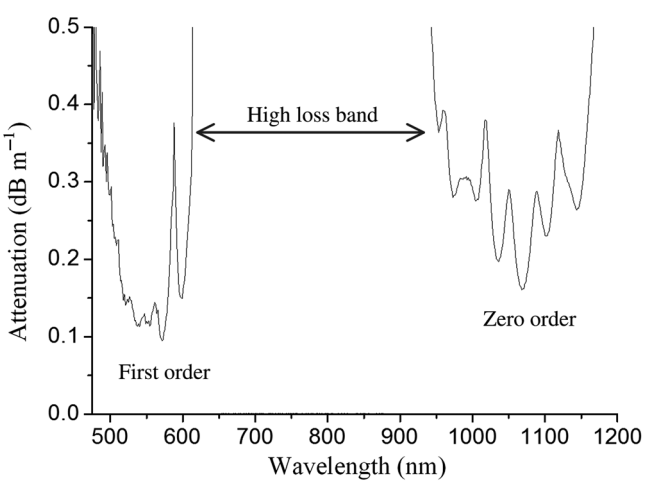

Fig. 3 Attenuation spectrum of zero-order NCF presented in this paper showing both the first- and zero-guidance bands.

3 Experimental Setup

The experimental setup is based on the dispersive Fourier transform spectroscopy and specifically based on methods previously reported.[19,20] This technique is based on measuring the phase difference between Fresnel reflections at the input and output surfaces of a fiber. However, in the case of the NCF, the core is hollow and there are no useable Fresnel reflections; hence, mirrors need to be introduced instead. For clarity, the measurement technique and, particularly, the data analysis used in these experiments are presented here in full.

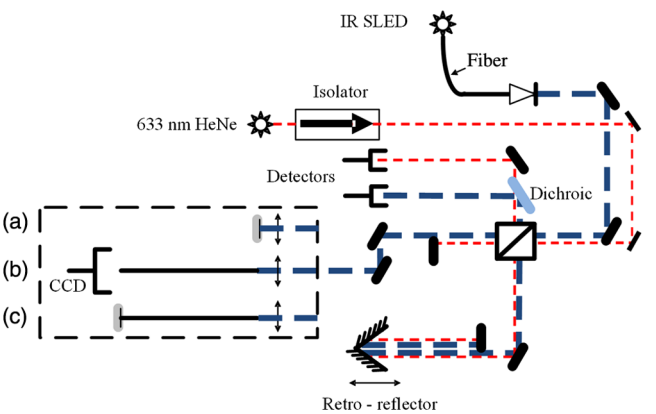

Fig. 4 Schematic of the scanning Michelson interferometer setup. A high pass dichroic mirror is used to separate the red and infrared beams before the detectors. A series of arrangements are used for the measurement arm at different stages of the experiment: (a) reference "front face" measurement, (b) alignment setup, and (c) "back face" measurement.

3.1 *Dispersion Measurement*

A ~300-mm length of fiber was used (the exact length was determined after the experiment) mounted between two microblocks with a very slight slack. Ideally the fiber would be kept straight to prevent intermodal coupling; however, some flexibility is necessary to allow for fine alignment of the coupling both into and reflecting back from the fiber end.

While intermodal coupling was observed in one of the fibers the effective refractive index of adjacent modes is sufficiently large enough to allow the interference from the modes to be spatially separated along the scanning arm allowing for an unambiguous measurement (see Fig. 8 and Sec. 3.2). Figure 4 shows a schematic of the setup based on a Michelson interferometer. An air bearing retroreflector is used to form the scanning arm. This provides a scan length

of up to 2 m due to the folded beam path. As the velocity of the retroreflector is not constant, a stabilized HeNe (633 nm) was used to measure the position of the scanning arm.

The HeNe light passes through an optical isolator, a pair of steering mirrors and is incident onto the beamsplitter. The transmitted light is reflected from a fixed reference mirror while the other passes through the retroreflector scanning arm. On recombination, the HeNe beams pass through a dichroic mirror and finally interfere on a silicon detector.

The optical source used for dispersion measurements was an Exalos EXS210063 SLED, centered at 1047 nm with a full width at half maximum (FWHM) bandwidth of 60.5 nm (coherence length $\sim 8\ \mu$m). This was coupled to 10 m of Nuferen 1060XP fiber which is single mode over this bandwidth and acts as a mode filter. An optical polarizer was used to fix the polarization of the source with respect to the test fiber at launch. At the beamsplitter, the IR beam is split into test and scanning arms. The scanning arm light passes through and is returned back by the scanning retroreflector. The test arm light, meanwhile, is coupled through a pair of alignment mirrors and then into the NCF via a microblock arrangement. An aspheric optic is used to couple into the fiber providing an numerical aperture (NA) match for the given NCF and the measured beam diameter of 0.85 mm (FWHM) (first-order NCF: ThorLabs C560TME-B, $f = 13.86$ mm, NA 0.03; zero-order NCF: ThorLabs A390TM-B, $f = 4.6$ mm, NA 0.09).

Measurement surfaces (Ag mirrors) were introduced to the system to provide reflection both with and without the fiber in place. For the reference measurements, a mirror was mounted to the microblock at the focus of the coupling optic such that the reflection is returned and recollimated by the focusing optic [Fig. 4(a)]. Alignment of the reference mirror is trivial due to the microblock arrangement; this surface is referred to as the "front face."

Alignment of the system to the fiber is more challenging. By use of a CCD and observing the output of the fiber, it was possible to dynamically adjust the coupling conditions to ensure primarily single mode transmission through the fiber [Fig. 4(b)]. This CCD can observe the far field and, using a 20× microscope objective, near field in transmission.

In the measurement arrangement, this mirror is moved into contact (butt-coupled) with the output of the NCF. This mirror is mounted on a x, y tilt mirror mount to facilitate alignment [Fig. 4(c)]. Alignment of the second reflective surface, referred to as the "back face," in contact with the NCF must be carefully adjusted to ensure the returned beam fills the fundamental mode as fully as possible. A high speed camera (Kodak EKTAPro 45401mx) was used at the position of the detectors (Fig. 4) to observe the far field and allow dynamic adjustment of the mirror-recoupling conditions. This camera was also used for Fourier imaging (cf. Sec. 3.2).

Data were acquired by a free running LeCroy 9354L 500 MHz oscilloscope recording the intensity at both the 1030 and 633 nm silicon detectors simultaneously. Up to 2.5 mm of scan data were acquired for each measurement, sufficient to include the complete interferogram from either the front or back reflection. At this rate, data were taken at ~1 nm increments with a single interferogram recorded in ~80 ms. As outlined in Sec. 4.1, multiple interferograms were recorded for each refection surface, a process taking ~2 min, and then combined and processed to calculate the dispersion as outlined in Sec. 4.1.

3.2 *Mode Identification*

As mentioned above, the fiber supports a small number of modes. For this experiment, the fiber length and the different effective refractive indices of these modes are sufficient for modes to appear separately within the scanned data. Although it can be assumed that the shortest path length (hence lowest effective refractive index) corresponds to the fundamental mode, we believed it necessary to verify this experimentally. This was accomplished by performing a Fourier analysis on the two-dimensional far-field image at the measurement point. A Kodak EKTAPro HS camera imaging at 40.5 kHz was used to image the interferograms at a sufficient rate to resolve the interferograms (this camera can also be used to aid alignment of the back face mirror). These data were then processed to provide an image of the interfering mode as outlined in Sec. 4.2. Note that this measurement was, by necessity, carried out separately from the dispersion measurement.

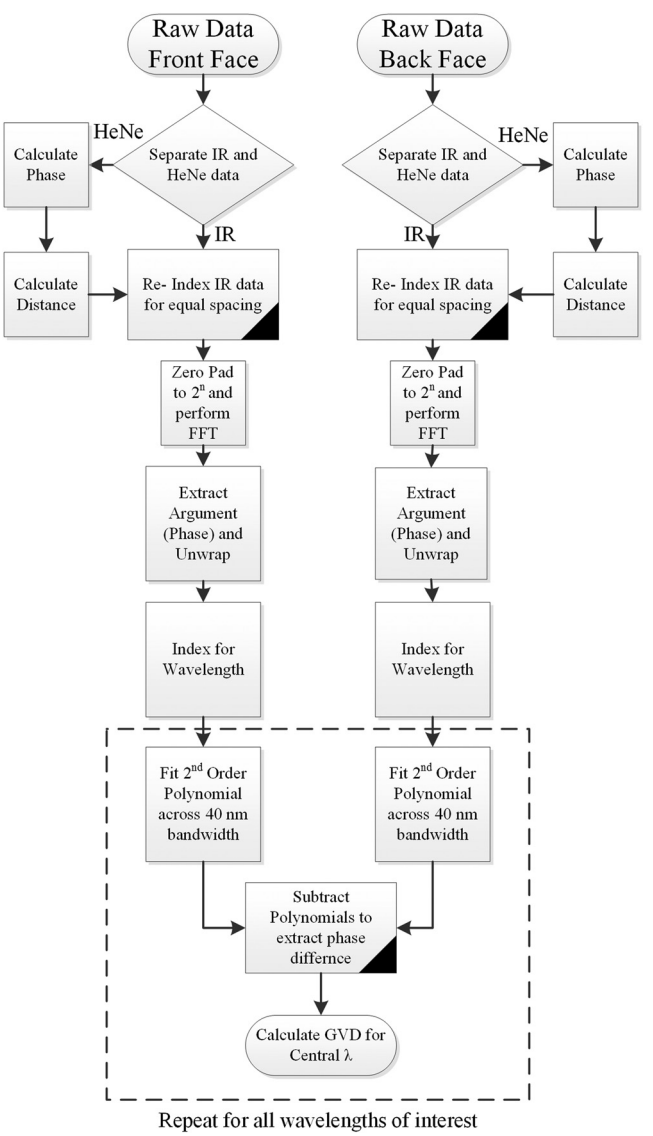

Fig. 5 Flow diagram of data processing process for a single measurement.

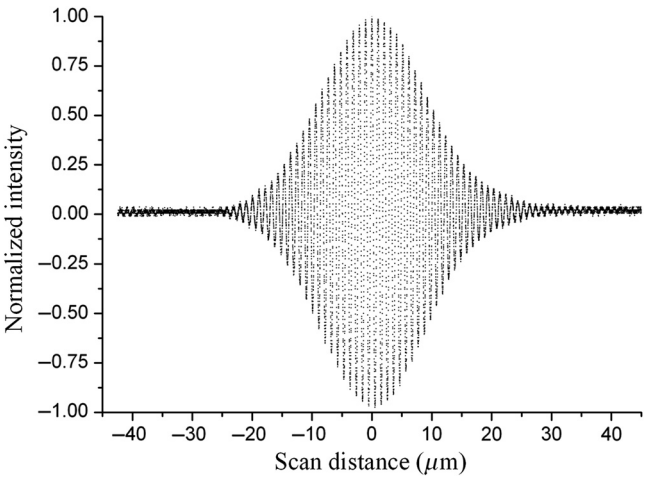

Fig. 6 Example interferogram from front face. NB scan distance has been zeroed to center of interferogram.

4 Data Processing

4.1 *Dispersion*

A flow chart of the data processing steps is presented in Fig. 5. To convert the collected data to a useable format, it was first necessary to interpolate and resample the IR intensity data to equal, known, scan distance steps. To do this, the HeNe data were used. Each individual fringe of the HeNe interferogram (i.e., π phase, $633/2$ nm) was fitted to a sinusoid and the phase extracted for each datum. This phase information was unwrapped over the whole dataset and converted to a distance, zeroed arbitrarily at the shortest scan length datum.

As the HeNe and IR data were acquired simultaneously on two channels of the oscilloscope this distance map can be applied directly to the IR data. A first-order interpolation of the IR dataset was calculated at equal distance intervals of 5 nm (this length is longer than the data spacing in the raw data but sufficiently short to provide ample data over each IR fringe to prevent aliasing).

In general, there may be more than one mode, and therefore more than one interferogram present in the data. In order to measure the dispersion of an individual mode, the data

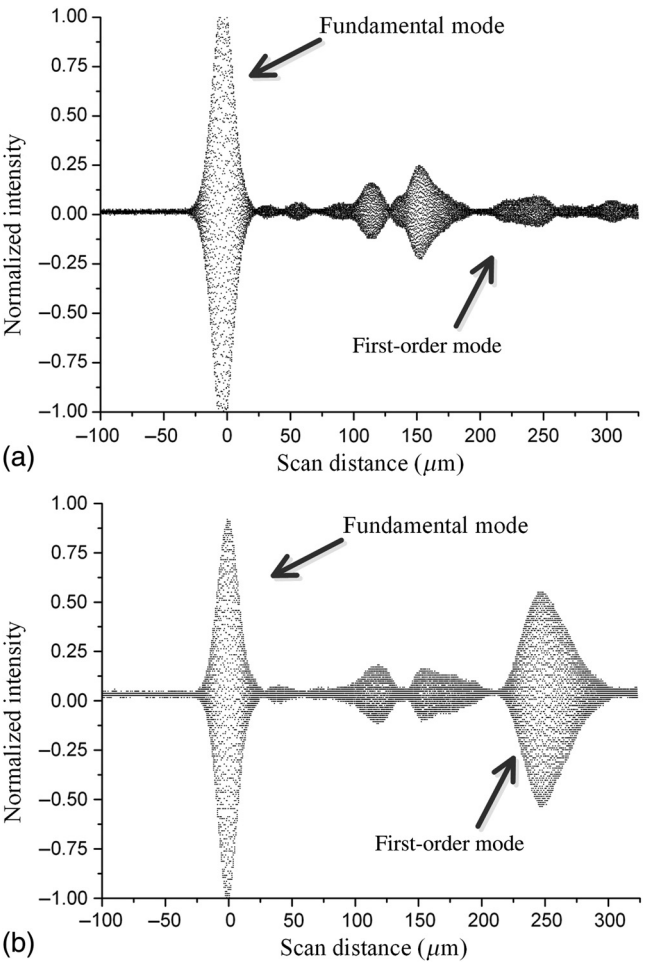

Fig. 8 Example interferogram from the back face for first-order NCF. NB zero path length difference has been centered to the fundamental mode. (a) Light coupled primarily into the fundamental mode and (b) significant coupling into the first-order mode.

were windowed. With the interferograms suitably windowed, the data were zero padded to the next 2^n dataset size and a fast Fourier transform (FFT) taken. The absolute components of the FFT correspond to intensity information, i.e., transmission spectrum at the two interfaces. This provides

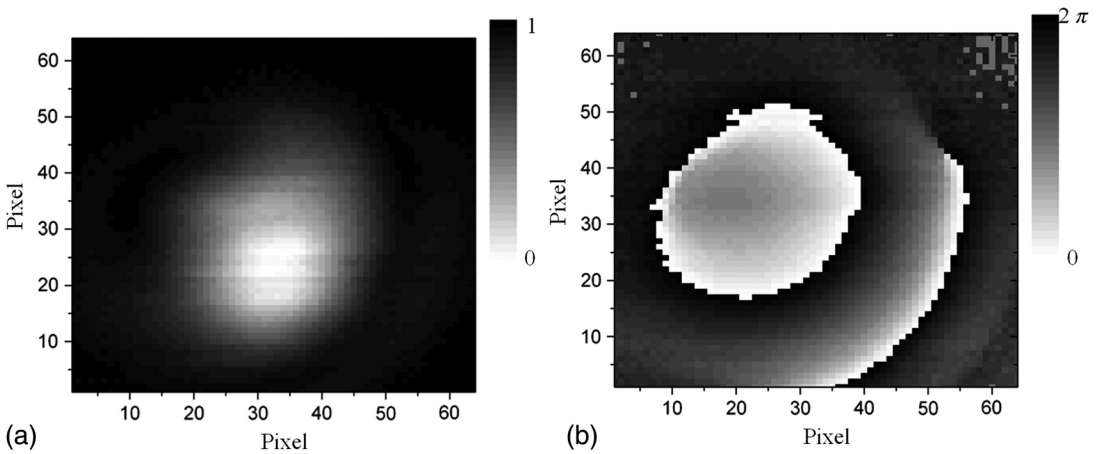

Fig. 7 Result of Fourier mode analysis for front face of first-order NCF: (a) intensity and (b) phase. A single maxima is visible in both images indicating a fundamental mode.

a useful check to determine if the system is working correctly. The argument components of the FFT correspond to the phase information and are therefore used to calculate the dispersion of the fiber.

To calculate the group velocity dispersion (GVD), the phase, as a function of angular frequency, is fitted to a second-order polynomial across a nominal bandwidth range. For these experiments, the bandwidth used corresponds to 40 nm, which is smaller than the FWHM of the source (60.5 nm). The phase is fitted to the second-order polynomial for the front and back faces independently. These phase equations are subtracted to determine the phase change across the fiber. The GVD between the two interfaces can then be calculated as

$$d = -\frac{\omega^2}{2\pi c}\frac{\partial^2 f[\Delta\theta]}{\partial^2 \omega^2}, \tag{1}$$

where d is the GVD, c is the speed of light, ω is the angular frequency, and f is the function describing the phase change due to the fiber. Taking the second derivative here eliminates the uncertainty due to an arbitrary zero phase from the unwrapping of the argument of the Fourier transform.

This provides the dispersion between the two interfaces; by dividing the path length within the fiber (twice the NCF length), the dispersion may be calculated as

$$d_{\mathrm{NCF}} = -\frac{d_{\mathrm{meas}}}{2l}, \tag{2}$$

where d_{NCF} is the GVD of the NCF, d_{meas} is the measured GVD between the two interfaces, and l is the length of the NCF under test. Care must be taken with the units to ensure a final result is given in $\mathrm{ps}\cdot\mathrm{nm}^{-1}\cdot\mathrm{km}^{-1}$. This value corresponds to the dispersion of the source at the central wavelength of the bandwidth used for the phase fit.

This process can be repeated for several fitted bandwidths to give the slope of the GVD within the overall bandwidth of the source. This process was repeated for 20 separate measurements for averaging and statistical error measurement.

4.2 *Fourier Imaging*

The data collected from the fast camera may be used to identify modes by measuring the shape of the mode actively interfering within each burst of the interferogram. This is achieved by windowing the data for a specific burst and examining the Fourier transform of the data collected by each individual pixel on the camera separately. Within the FFT, there is a peak associated with the fringes moving across the pixel. By plotting the magnitude of both the absolute (intensity) and argument (phase) of this peak for each pixel, an image of the interfering mode can be reconstructed. More details of this process can be found in Ref. 21.

5 Results

5.1 *First-Order NCF*

Figure 6 shows an example resampled interferogram from the front face. This shows a clear single mode, single

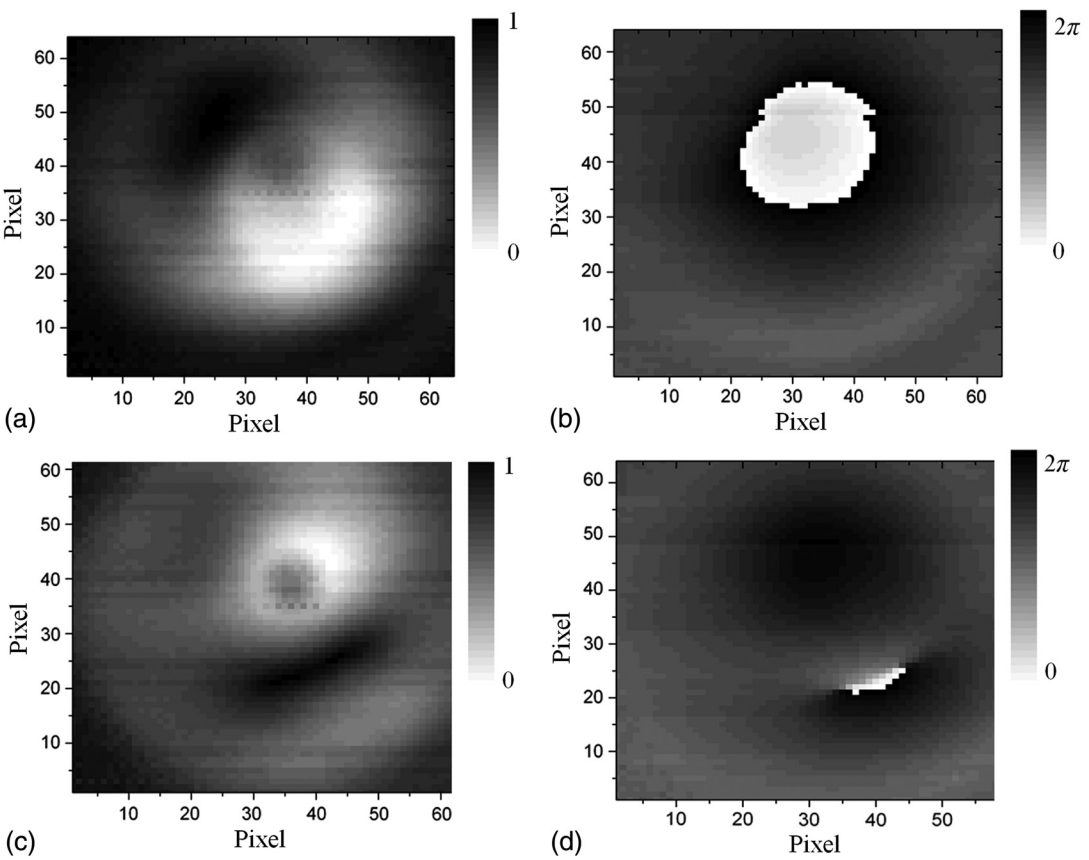

Fig. 9 Results of Fourier mode analysis for front face of zero-order NCF: (a) intensity and (b) phase of fundamental mode, (c) intensity and (d) phase of first-order mode.

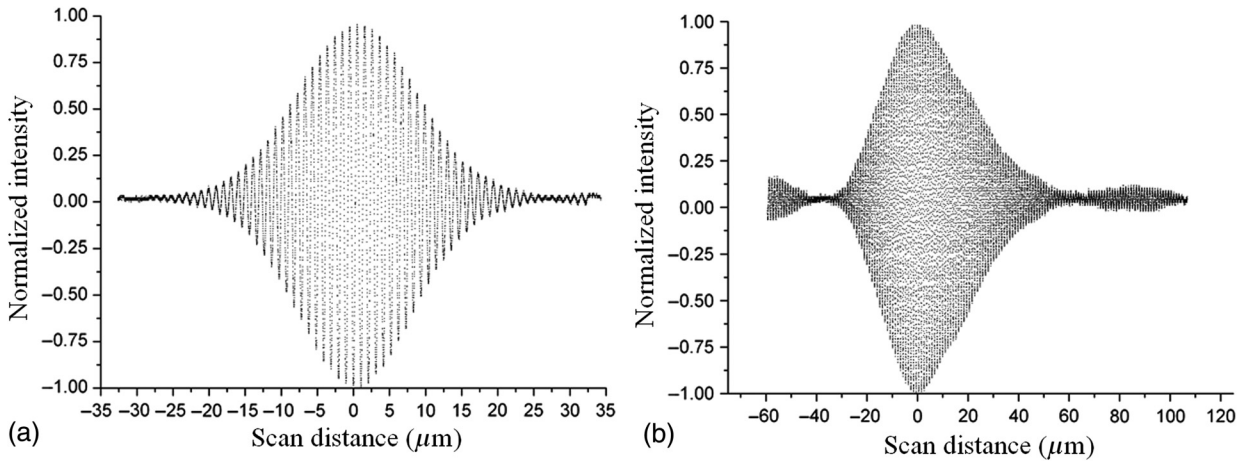

Fig. 10 Example windowed interferograms from back face of (a) fundamental mode and (b) first-order mode of first-order NCF. NB zero path length difference is zeroed on the respective modes.

interface, interference burst and Fig. 7 shows the result of the Fourier analysis which also demonstrates a single mode.

Figure 8 shows example resampled interferograms from the back face. This indicates that a series of modes have been coupled into the NCF. The first (left hand) interference burst is expected to correspond to the fundamental mode, since it has the lowest effective refractive index. There is a second clear mode at an effective path length of $+240$ μm from the fundamental and a series of less well defined low power modes between them. It was found that the proportion of radiation coupled into each mode could be altered by changing the coupling conditions into the fiber as can be seen by comparing Figs. 8(a) and 8(b).

The Fourier mode analysis, Fig. 9, confirms that the left-hand mode is the fundamental while the right-hand mode is a first-order mode. The dispersion of both the fundamental and first-order modes may be measured separately by windowing data suitably. Figure 10 shows the windowed data corresponding to the fundamental and first-order modes.

The length of the fiber was measured using a position tracking microscope as 296.2 mm, the error in this case can be assumed to be insignificant (at worst ± 0.5 mm) since the error in the GVD dominates. Figure 11 shows the result of calculated GVD taken from 20 separate measurements of both the fundamental and first-order modes. The mean GVD and 1-sigma error were measured to be 2.17 ± 0.25 ps $\cdot$ nm^{-1} $\cdot$ km^{-1} for the fundamental mode and 4.69 ± 0.17 ps $\cdot$ nm^{-1} $\cdot$ km^{-1} for the first-order mode, both at 1030 nm.

5.2 *Zero-Order NCF*

Figure 12 shows an example back interferogram from this fiber which is single mode. The Fourier analysis of the interfering mode confirms that the mode is a fundamental mode (Fig. 13).

As only one mode is present, the widowing conditions for the Fourier transform are not critical. The length of the fiber was measured using a microscope as 542.4 mm, the error in this case can be assumed to be insignificant (at worst ± 0.5 mm) since the error in the GVD dominates. Figure 14 shows the results of the GVD calculation. Results are the mean of 20 measurements with a 1-sigma error. The dispersion at 1030 nm is 3.81 ± 0.03 ps $\cdot$ nm^{-1} $\cdot$ km^{-1}.

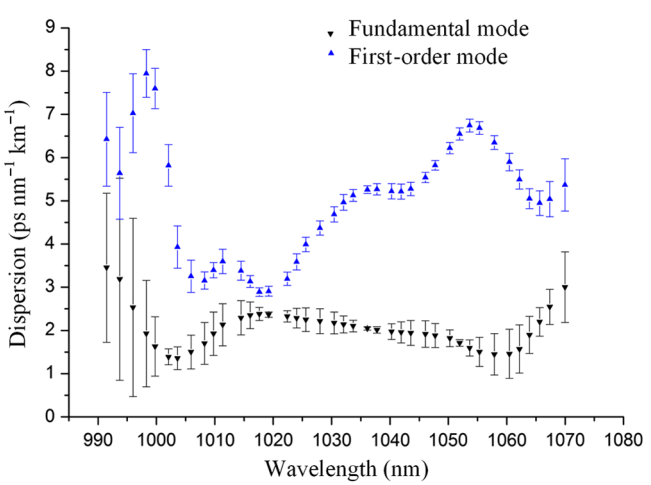

Fig. 11 Calculated CVD of the first-order NCF. Results are the mean of 20 separate measurements with error bars corresponding to 1-sigma error.

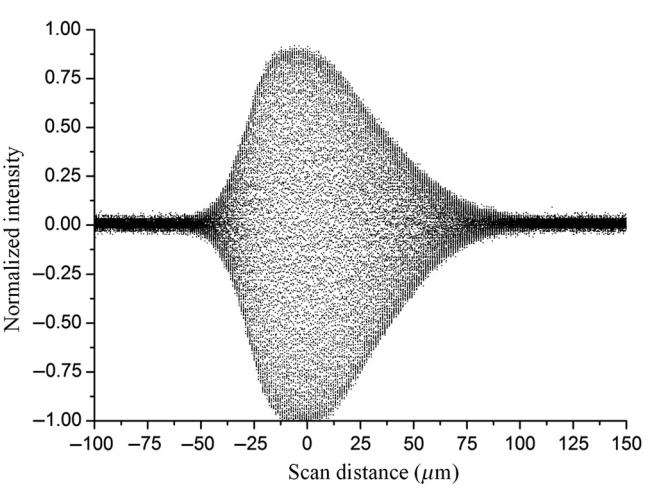

Fig. 12 Example interferogram from the back face for the zero-order NCF. Only one fundamental mode is present in this fiber.

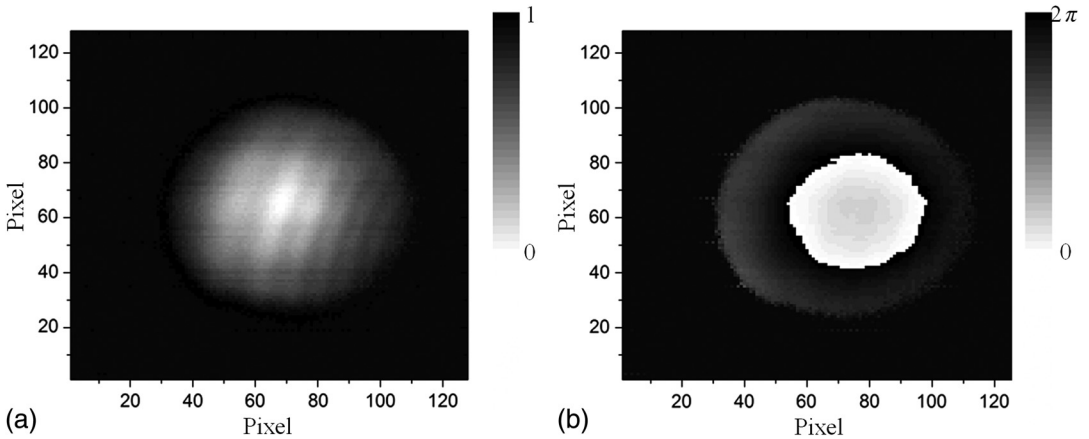

Fig. 13 Results of Fourier analysis of the mode measured in the back interferogram for the zero-order NCF: (a) intensity and (b) phase. The mode is fundamental.

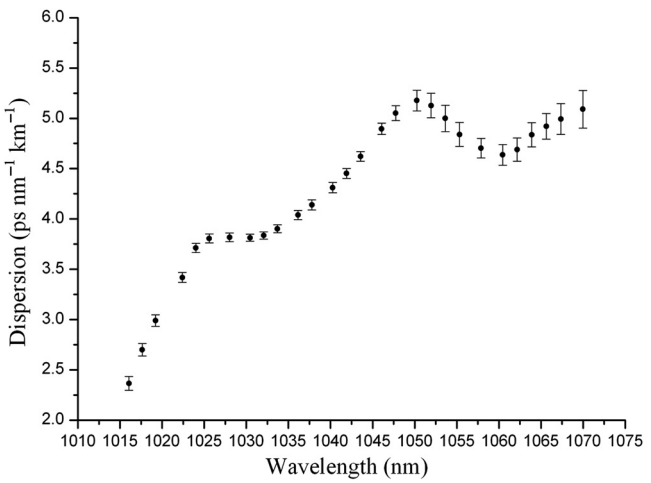

Fig. 14 Calculated GVD of the zero-order NCF. Results are the mean of 20 separate measurements with error bars corresponding to 1-sigma error.

6 Conclusions

Both fibers exhibit low anomalous dispersion. In the 1030-nm fiber, the dispersion of the fundamental mode is, as expected, lower than the first-order mode. Likewise the dispersion of the 515-nm fiber is higher than the 1030-nm fiber, and most likely this is a result of the larger overlap between core mode and (glass) cladding as a result of a smaller core. Although the measured dispersion curves are nonmonotonic, this behavior may potentially be correlated with local loss deatures seen in the transmission spectra in Figs. 2 and 3, due to the complex guidance mechanics of these fibers, e.g., coupling between cladding and fundamental modes linked to, wavelength-dependent loss, variations in the overlap between the propagating mode and glass[22] (and hence the GVD), or even localized degradation of the fiber structure. Further discussion of this correlation may be found in Ref. 23; however, more efforts are needed to further explore this topic which is beyond the scope of this paper.

Overall the dispersion is low, illustrating the feasibility for guiding high peak power, ultrashort pulses for industrial and telecommunication applications.

Acknowledgments

This work was funded by the UK Engineering and Physical Sciences Research Council under Grant Nos. EP/I0235+X/1 and EP/I011315/1.

References

1. F. Poletti et al., "Towards high-capacity fibre-optic communications at the speed of light in vacuum," *Nat. Photonics* **7**, 279–284 (2013).
2. A. Kuhn et al., "Optical fibre beam delivery of high-energy laser pulses: beam quality preservation and fibre end-preparaion," *Opt. Lasers Eng.* **34**(4–6), 273–288 (2000).
3. J. Parry et al., "Analysis of optical damage mechanisms in hollow-core waveguides delivering nanosecond pulses from a Q-switched Nd:YAG laser," *Appl. Opt.* **45**(36), 9160–9167 (2006).
4. J. Parry et al., "Optical fiber array for the delivery of high peak-power laser pulses for fluid flow measurements," *Appl. Opt.* **46**(17), 3432–3438 (2007).
5. J. D. Shephard et al., "High energy nanosecond laser pulses delivered single-mode through hollow-core PBG fibers," *Opt. Express* **12**(4), 717–723 (2004).
6. B. Beaudou et al., "Millijoule laser pulse delivery for spark ignition through kagome hollow-core fiber," *Opt. Express* **37**(9), 1430–1432 (2012).
7. F. Emaury et al., "Beam delivery and pulse compression to sub-50 fs of a modelocked thin-disk laser in a gas-filled Kagome-type HC-PCF fiber," *Opt. Express* **21**(4), 4986–4994 (2013).
8. B. Deboard et al., "Ultra low-loss hypocycloid-core Kagome hollow-core photonic crystal fiber for green spectral-range applications," *Opt. Lett.* **39**(21), 6245–6248 (2014).
9. S. Pricking et al., "Hollow core fiber delivery of sub-ps pulses from a TruMicro 5000 Femto edition thin disk amplifier," *Proc. SPIE* **9356**, 935602 (2015).
10. P. Jaworski et al., "High energy green nanosecond and picosecond pulse delivery through a negative curvature fiber for precision micro-machining," *Opt. Express* **23**(7), 8498–8506 (2015).
11. P. Jaworski et al., "Picosecond and nanosecond pulse delivery through a hollow-core negative curvature fiber for micro-machining applications," *Opt. Express* **21**(19), 22742–22753 (2013).
12. F. Yu and J. C. Knight, "Spectral attenuation limits of silica hollow core negative curvature fiber," *Opt. Express* **20**(10), 11153–11158 (2012).
13. A. D. Pryamikov et al., "Demonstration of a waveguide regime for a silica hollow-core microstructured optical fiber with a negative curvature of the core boundary in the spectral region >3.5 μm," *Opt. Express* **19**(2), 1441–1448 (2011).
14. A. Urich et al., "Silica hollow core microstructured fibres for mid-infrared surgical applications," *J. Non-Cryst. Solids* **377C**, 236–239 (2013).
15. A. Urich et al., "Flexible delivery of Er:YAG radiation at 2.94 μm with negative curvature silica glass fibers: a new solution for minimally invasive surgical procedures," *Biomed. Opt. Express* **4**(2), 193–205 (2013).
16. N. M. Litchinitser et al., "Antiresonant reflecting photonic crystal optical waveguides," *Opt. Lett.* **27**(18), 1592–1594 (2002).
17. A. N. Kolyadin et al., "Negative curvature hollow-core fibres: dispersion properties and femtosecond pulse delivery," *Phys. Proc.* **73**, 59–66 (2015).

18. A. Sherlock et al., "Tunable fiber-coupled multiphoton microscopy with a negative curvature fibre," *J. Biophotonics* **9**(7), 715–720 (2016).
19. A. A. Flavin et al., "Combined temperature and strain measurement with a dispersive optical fiber Fourier-transform spectrometer," *Opt. Lett.* **19**(24), 2167–2169 (1994).
20. M. J. Gander et al., "Experimental measurement of group velocity dispersion in photonic crystal fibre," *Electron. Lett.* **35**(1), 63–34 (1999).
21. P. Nandi et al., "Characterization of a photonic crystal fiber mode converter using low coherence interferometry," *Opt. Lett.* **34**(7), 1123–1125 (2009).
22. W. Belardi and J. C. Knight, "Effect of core boundary curvature on the confinement losses of hollow antiresonant fibres," *Opt. Express* **21**(19), 21912–21917 (2013).
23. G. K. Alagasev et al., "Impact of geometrical paramaters on optical properties of negative curvature hollow-core fibers," *Laser Phys.* **25**, 055101 (2015).

Richard M. Carter is currently a research associate at the Institute of Quantum Sciences, Heriot-Watt University, Edinburgh. He received his MPhys (Hon) degree in physics from Edinburgh University in 2005, his Msc degree in photonics and optoelectronics from St. Andrews and Heriot-Watt University in 2007, and his PhD from Heriot-Watt University in 2012, where he is now working on fiber optics for high-power delivery and laser-based production processes.

William N. MacPherson is an associate professor of physics and a member of the Applied Optics and Photonics Research Group at the School of Engineering and Physical Sciences, Heriot-Watt University. His research interests are centered around the application of optical and fibre-optic techniques for measurement and instrumentation. He has published over 100 journal and conference papers in this area. Ongoing research is looking at subsea sensor applications and uses of fibres for optical tweezing.

Piotr Jaworski graduated from the Wroclaw University of Technology in 2011 with his MSc degree in electronics and telecommunication. After that he moved to Heriot-Watt University where he worked on high-peak power pulse delivery through hollow-core microstructured fibres and obtained his PhD in physics in 2015. Currently, he is a research engineer in Wroclaw Research Centre EiT+ and his work is focused on laser-based spectroscopy.

Fei Yu received his BS and MS degrees in physics electronics from Beijing Institute of Technology, Beijing, China, in 2008 and 2010, respectively, and his PhD in optics from the University of Bath, Bath, UK, in 2014. Since 2014, he has been working as a research officer at the University of Bath. His research interests include optical-fiber design and applications.

Rainer Beck graduated from Heriot-Watt University with his MPhys (hons) degree in 2007 and his PhD on "Adaptive Optics for Laser Processing" in 2011. He gained industrial experience working in R&D on automotive display applications and as product manager for surgical lasers. In 2014, he returned to Heriot-Watt University and his research interests are based around high precision additive and subtractive laser processing, as well as minimally invasive laser surgery techniques for cancer treatment.

Jonathan D. Shephard received his engineering degree from Cambridge University in 1994, worked within R&D at Pilkington Plc in 1995 and was awarded his MSc (Eng) degree with distinction in 1996 and PhD in 2000 on mid-IR transmitting glasses from the University of Sheffield. He moved to Heriot-Watt University in 2003 and is now an associate professor within the Institute of Photonics and Quantum Sciences developing fibres and laser processes for applications in manufacturing and medicine.

Duncan P. Hand has been carrying out research in optical fibers for 30 years, first, at the University of Southampton before moving to Heriot-Watt University in 1991, where he is now a professor of applied photonics. In addition to work on fiber optics, he leads research activity in applications of high-power lasers and is currently director of the 5-university EPSRC Centre for Innovative Manufacture in Laser-Based Production Processes.